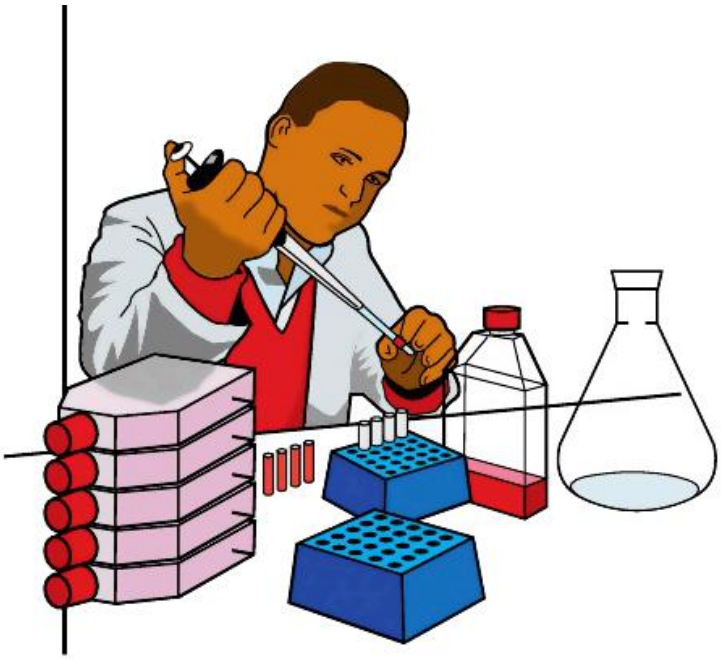

Experimental Details

Chapter 4 Experimental Details

Synthesis techniques for ionization radiation detector materials have been discussed and summarized in chapter 2. In the present thesis work, the synthesis routes for the preparation of such nanorods have been developed for cost-effectiveness and large productions. In section 4.1, sol-gel seeding followed by dip coating used to synthesize scintillator materials has been discussed. It includes the preparation of ZnO:Ga nanorods and composite scintillator for alpha radiation detection. Synthesized materials are characterized for their structural, morphological, optical and luminescence properties using various characterization equipment as described in section 4.2. Further, nanorod /composite scintillators are described in section 4.3 which are coupled with photomultiplier tube and multichannel analyzer (MCA) to develop detector for alpha radiation.

4.1 Nanorod/Composite Preparation Techniques

4.1.1 Low-Temperature Hydrothermal Method for Nanorods

The low-temperature hydrothermal method is the simplest, cost-effective and energy-saving method for the growth of ZnO nanorods at low temperature ~ 90-95 ^{0}C in a solution. It consists of fabrication of seed layer of ZnO on a transparent substrate using spin coating a gel of ZnO, prepared using sol-gel method, followed by growth of nanorods over these seed by dipping the substrate in an aqueous solution containing zinc ions, doping ions and weak base working as hydrolyzer and finally annealing of the substrate. The process of ZnO:Ga nanorods over FTO glass substrate is schematically summarized in figure 4.1.

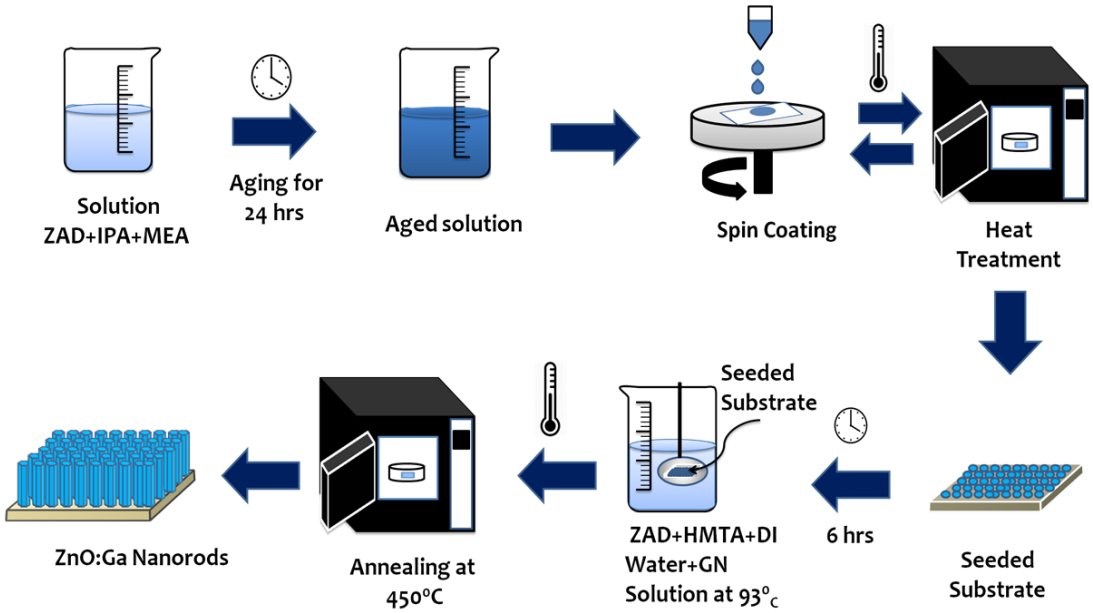

Figure 4.1: Preparation of ZnO:Ga Nanorods using low-temperature hydrothermal method

4.1.1.1 Seeding

Zinc acetate dehydrates dissolved in mono ethylamine and isopropyl alcohol, followed by magnetic stirring to get a uniform solution. The solution is aged at room temperature for 24 hours. A layer is formed on the glass substrate using spin coating. The spin-coated substrate is then heated up to 450 ^{0}C, leading to the formation of ZnO seeds over the substrate. The substrate is again coated with gel and heated. The process repeated until desired thickness of seed was obtained on the substrate. The chemical reaction involved in the seeding process is

schematically summarized in figure 4.2. Zinc acetate dissolved in IPA lead to the formation of zinc monoacetate and other ions. Zinc monoacetate form a complex with MEA. Hydrolysis of this complex results in the formation of zinc hydroxide. Zinc hydroxide decomposes in ZnO upon heating (Nehmann et al., 2014)

$$Zn(OAc)_2 + IPA \xrightarrow{IPA} Zn(OAc)^+ + Ac^- + H^+ + OH^-$$

$$Zn(OAc)_2 + OH - CH_2 - CH_2 - NH_2 \rightarrow Zn\,[OH - CH_2 - CH_2 - NH_2] + Ac^- + H^+ + OH^-$$

$$Zn\,[OH - CH_2 - CH_2 - NH_2] \xrightarrow{hydrolysis} Zn(OH)_2 + OH - CH_2 - CH_2 - NH_2$$

$$Zn(OH)_2 \xrightarrow{Heat} ZnO + H_2O$$

4.1.1.2 ZnO:Ga Nanorods Formation

After the seeding process, the substrate is dipped in an aqueous solution containing Zinc acetate, Gallium nitrate, hexamethylenetetramine (HMTA) kept at 90-95 ^{0}C. HMTA reacts with water molecules to produce OH^- ions by hydrolysis process, which reacts with Zn^{+2} ions provided by zinc acetate and dopant Ga^{+3} ions to form $Ga_x\ Zn_{1-x}\ (OH)_2$, which decomposes to GZO upon heating ~400 ^{0}C. The chemical reaction involved in the process of ZnO:Ga nanorod growth is listed below;

$$(CH_2)_6N_4 + 6H_2O \leftrightarrow 4NH_3 + 6HCHO$$

$$NH_3 + H_2O \leftrightarrow NH_3 \cdot H_2O$$

$$NH_3 \cdot H_2O \leftrightarrow NH_4^+ + OH^-$$

$$(1-x)Zn^{2+} + xGa^{3+} + 2OH^- \leftrightarrow Zn_{1-x}Ga_x(OH)_2$$

$$Zn_{1-x}Ga_x(OH)_2 \leftrightarrow Zn_{1-x}Ga_xO + H_2O$$

Precursor concentration, temperature and growth time are critical parameters that control the reactions.

4.1.2 Composite Scintillator Preparation

Composite scintillator film prepared by the solution mixing process. ZnO 99.995% microparticles (<5 μm) mixed with fine granules of polystyrene and then mixed with solvent toluene. The mixture is thoroughly stirred till the uniform mixing as milky white solution is obtained. Few drops of this solution are then poured and sandwiched between quartz substrate and then slide relative to each other to get the ZnO/PS layer on both substrates. Drying these substates for 12 hrs at room temperature leads to evaporation of toluene and ZnO/PS film is obtained on the glass substrate. To prepare ZnO-^{6}LiF/PS composite, ^{6}LiF in desired quantity added with ZnO. The process of preparation of ZnO/Polystyrene composite is shown in figure 4.2.

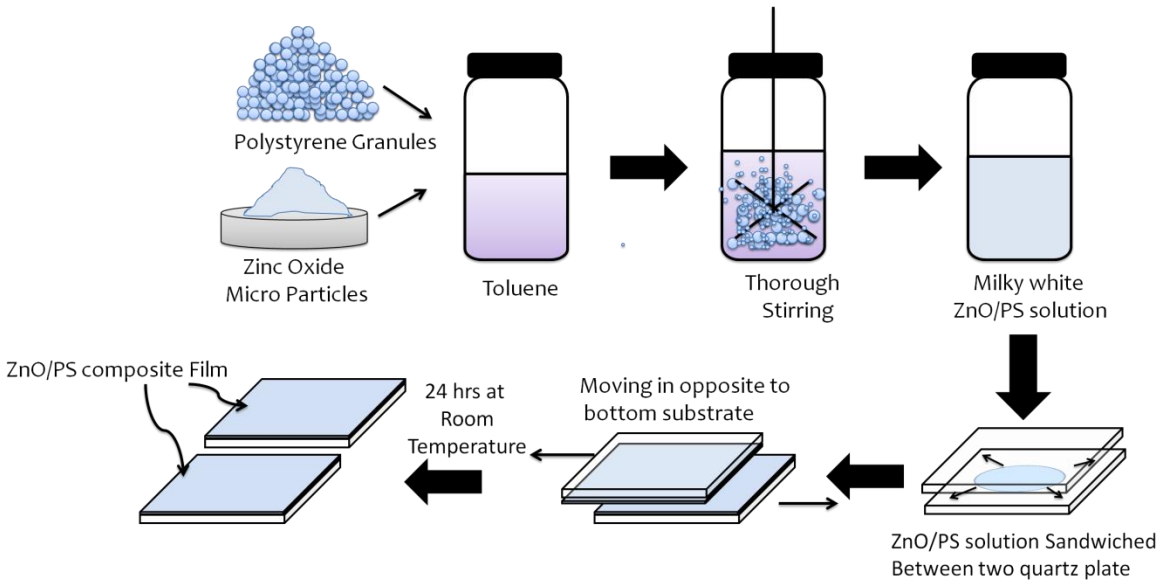

Figure 4.2: Schematic diagram of preparation zinc Oxide-Polystyrene Composite scintillator film

4.2 TiO_2 Nanorod Preparation using Hydrothermal Method

TiO_2 nanorods over FTO glass substrate are prepared using the hydrothermal method. FTO glass substrate is seeded with TiO_2 and then TiO_2 nanorods are grown over it. To make a seed layer, a solution of Titanium Tetraisopropoxide ($Ti\{OCH(CH_3)_2\}_4$) in IPA is prepared. Few drops of the solution are then spin-coated over the FTO substrate. The coated substrate is then annealed at 500 ^{0}C for 2 hrs to obtain a TiO_2 seeded substrate. Following reaction occurs in the seeding process

$$Ti\{OCH(CH_3)_2\}_4 + 4(CH_3)_2CHOH \rightarrow Ti(OH)_4 + 4(CH_3)_2CHO$$

$$Ti(OH)_4 \xrightarrow{500^0C} TiO_2 + 2H_2O$$

To grow TiO_2 nanorods over the seeded substrate, a solution of HCl and DI water (HCl: DI=1:1) were mixed in a Teflon-lined autoclave and stirred for 10 minutes with a magnetic stirrer. Then Titanium isopropoxide was added in 50 mM concentrations and stirred for 30 minutes. The seeded substrate is kept in the autoclave with an angle of 45° against the wall. The autoclave was kept in a hot air oven for 8h at 160°C. After complete reaction, the autoclave was taken outside the oven and cooled down to room temperature. The FTO glass substrate was washed with DI water and dried in air to get TiO_2 nanorods over the FTO substrate. The process of preparation of TiO_2 nanorods is schematically shown in figure 4.3.

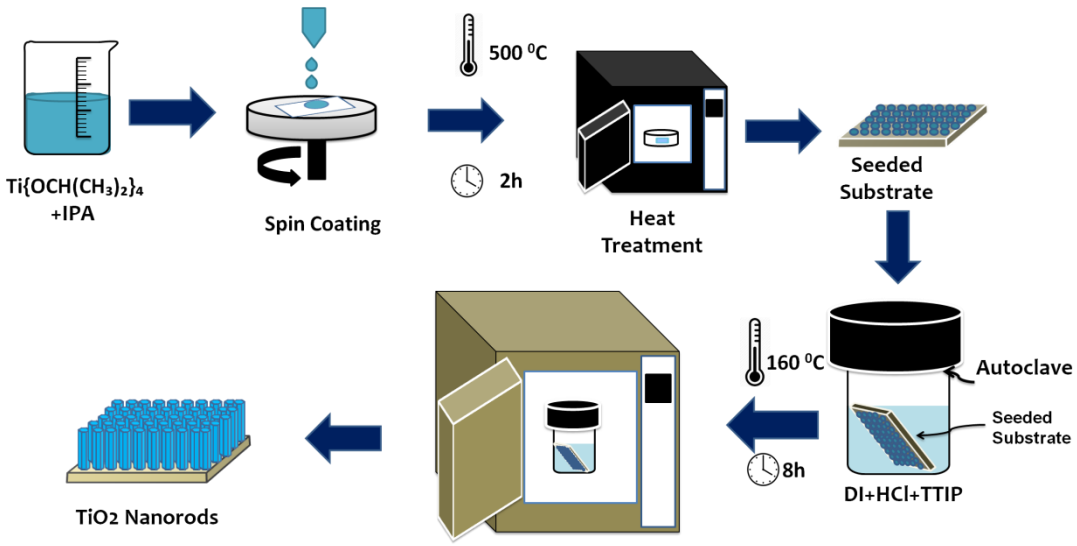

Figure 4.3: Schematic Diagram of TiO_2 nanorod synthesis on FTO glass substrate

4.3 Sample Characterization Techniques

After fabrication of nanorods/composites, the physical, micro-structural, optical and luminescence, scintillation, electrical properties are investigated to understand their structural evolution together with structure-property correlation. Several characterization techniques are explored to understand the material and radiation sensing properties such as structural, optical, electrical, luminescence and scintillation properties. These techniques include X-ray diffraction (XRD), Scanning Electron Microscopy (SEM), Photo-luminescence, Radioluminescence, UV-Vis-NIR spectroscopy, Raman spectroscopy, I-V Characterization, radiation-induced scintillation measurement. The basic principle of these techniques and description of the respective equipment used to characterize the developed radiation detector Nanorods/composites is discussed in the following section.

4.3.1 X-ray Diffraction (XRD)

X-ray diffraction is a characterization technique used to identify the crystal phases of the materials. X-rays are high-energy electromagnetic radiation with a typical wavelength ~0.01-100 A^0 produced during a collision between metal targets and high-speed accelerated electrons. These rays have the property of diffraction from atomic planes. X-ray diffraction was first invented in 1912 and since it was extensively used for structural characterization, especially the crystallographic structure, crystallinity and more specifically crystallite size. An X-ray tube consists of electrodes and a high voltage difference is applied across them to accelerate the electrons from the cathode and to fall on the target (anode) (figure 4.4a). Two types of X-rays are generated (i) continuous X rays due to slow down of electron in the target and (ii) characteristics X-ray, monochromatic x rays emitted due to transition to higher orbit electron to lower orbit because of the vacancy created by accelerated electrons (figure 4.4b)

X-ray diffraction spectrometer consists of X-ray tube for generation of x rays; soller slit for collimation of X-ray beam; Sample holder for placing the sample under investigation and detector for monitoring the diffracted X rays (figure 4.4 c). X-rays incident on the sample got diffracted by the atomic planes of the material and the interference pattern is obtained according to Bragg's law ($n\lambda = 2d \sin\theta$); where n is the order of diffraction, λ is the wavelength

of X-ray used, d inter planer spacing. The inter-planer spacing is a function of miller indices h,k,l and is different for different phases resulting in peaks at certain fixed angles. This principle is used to identify the phases of the materials (Leng, 2013) In our studies, we used Bruker's D8 Advance Powder X-ray diffractometer (figure 4.4 d), which employs a characteristic Cu-kα wavelength of 1.54 Å as a source of X-ray radiation.

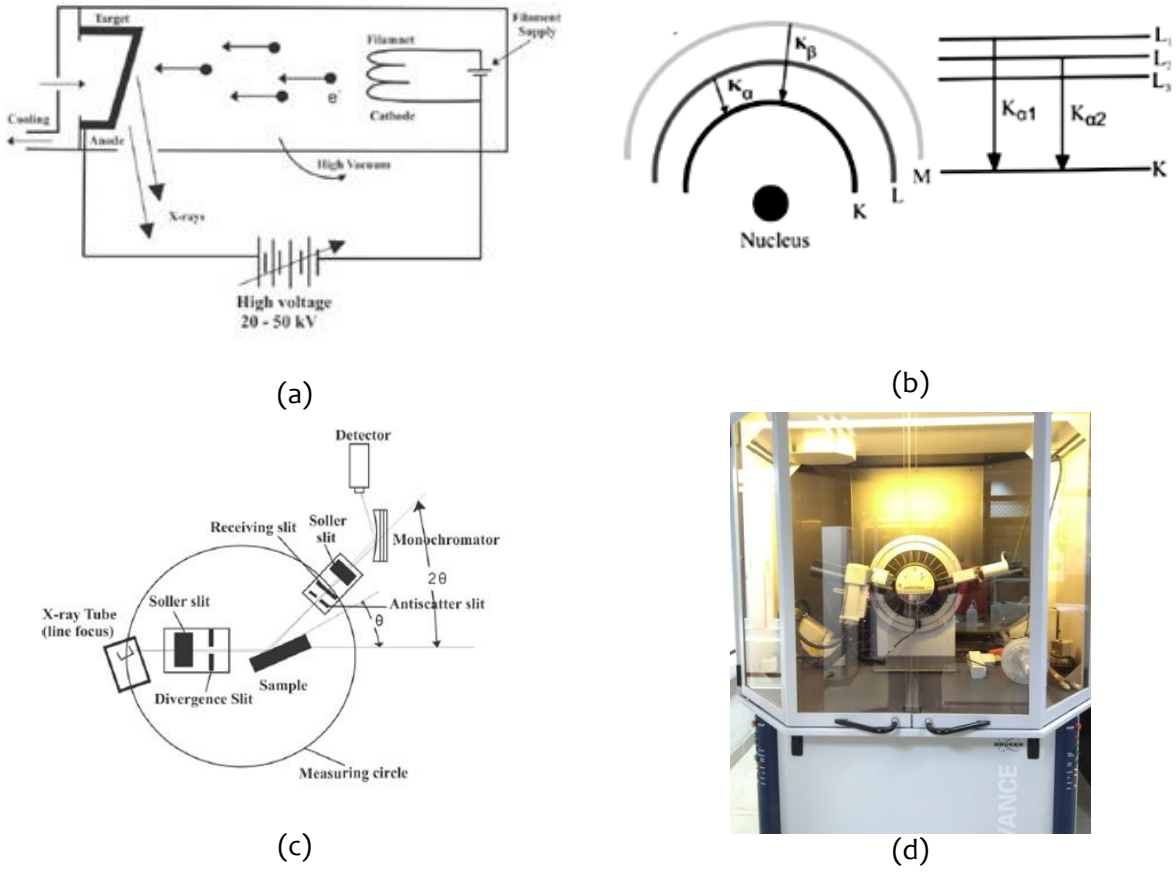

Figure 4.4 : (a) Schematic of X-ray tube structure and (b) schematic characteristics X-ray generation. (c) Schematic of the geometrical arrangement of X-ray diffractometer(Source: Leng, 2013) (c) Bruker's D8 Advance Powder X-ray diffractometer at IITJ

4.3.2 Scanning Electron Microscope (SEM)

Scanning Electron Microscopy (SEM) is used for microstructure characterization of any material such as surface and grain morphology of the sample. This method utilizes the beam of electrons interacting with sample material, generating secondary electrons or backscattered electrons, which contain surface morphology information. An image is created based on these emitted secondary electrons. Electron microscope consists of lanthanum bromide (LaB_6) or a field emission tip for the generation of electrons. The emitted electrons are brought to a focus or crossover with a Wehnelt electrode assembly aid. Electromagnetic lenses are then employed to de/magnify the cross-over and focus the electron probe on the sample's surface. Two to four electromagnetic lenses are used according to gun design for focusing arrangement. It is desirable to provide the final lens with a magnetic stigmator to correct astigmatism, which would otherwise increase the spot size. The narrow electron beam scans the surface of the

sample with the aid of a set of x and y deflecting coils. As a result of the simultaneous application of saw-tooth type wave currents to the two sets of coils, the beam can be moved along a diagonal path. The detected secondary electrons will be captured by CRT display in the form of an image. In this way, a complete picture of the object is displayed, which can be recorded (figure 4.5a.) In our studies, the samples' qualitative elemental analysis was done using Carl Zeiss EVO 18 scanning electron microscope (figure 4.5b).

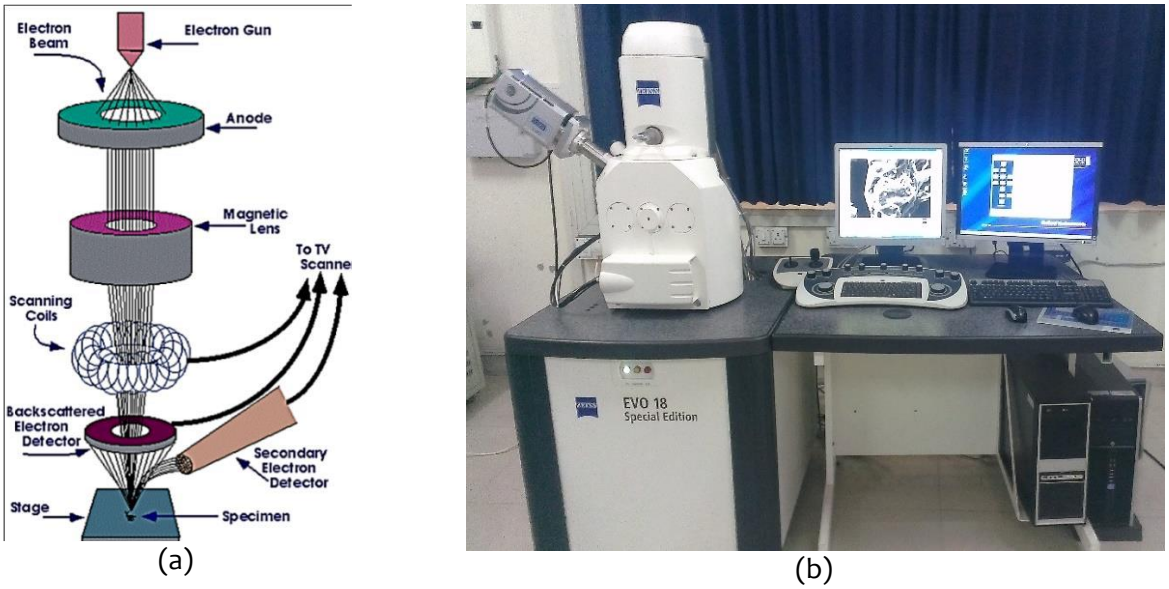

Figure 4.5: (a) Schematic of different component of scanning electron microscope (b) Carl Zeiss EVO18 System at IITJ

4.3.3 Photoluminescence Spectro-fluorometer

Spectro-fluorometer is an instrument to characterize the photo-luminescence properties of a sample. It utilizes a source of UV radiation such as Xe source ~150 Watt emitting 200-750 nm UV light for excitation of the sample. The light emitted by the Xe source is allowed to pass through the monochromator utilizing grating with ~1800 lines/mm, dividing the light in different wavelengths and then reaching a sample for excitation. The emitted luminescence light is again passed through the emission monochromator for measurement with photomultiplier tube (PMT) at the end. A beam splitter is used to correct temporal fluctuation in excitation light intensity, which divides the monochromatic light in two and feeds one to a secondary PMT measuring the intensity of monochromatic light used to rescale emission intensity measured by primary PMT. Figure 4.6a shows the schematic diagram of the optical design of Spectro-fluoro-meter and JASCO-6500 Spectro-fluorometer used in the study is shown in figure 4.6b.

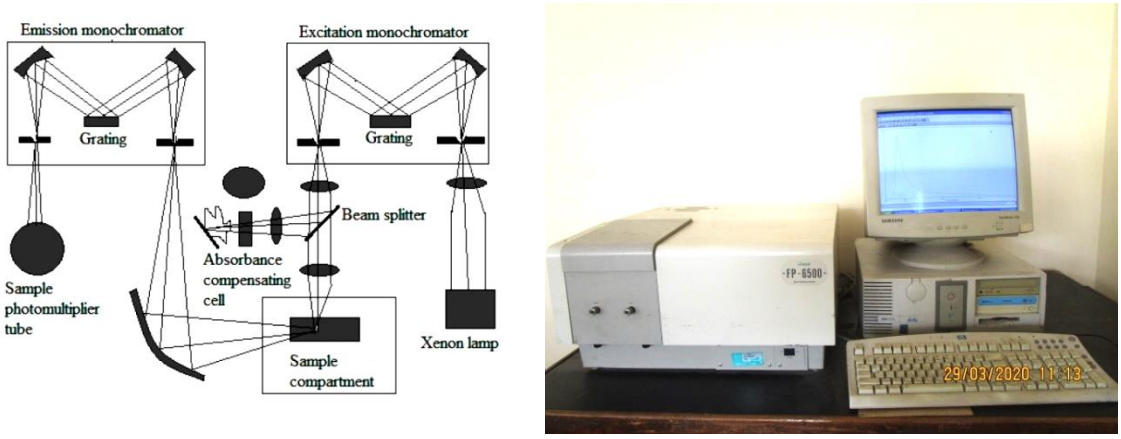

Figure 4.6: (a) Schematic diagram optical design of Spectro-fluorometer (b) JASCO-6500 Spectrofluorometer

4.3.4 Raman Spectroscopy

Raman spectroscopy is an important technique used to investigate structural and molecular information in terms of phonon vibrational spectrum for a material. It is based on the inelastic scattering of monochromatic light with the material. The monochromatic light source used is a laser source. The in-elastically scattered photons have frequency shift in the higher and lower side with respect to the original monochromatic frequency. This inelastic scattering of light from a material is called the Raman Effect. This Raman shift given by Eq. (3.4) provides information about vibrational, rotational and other low-frequency transitions in molecules. Therefore, it is a powerful tool to identify the chemical composition and structure of a material.

$$\Delta w = (1/\lambda_o - 1/\lambda_1)$$

Where Δw is the Raman shift (wavenumber), λ_o and λ_1 are excitation and Raman wavelengths, respectively. After inelastic scattering, if the scattered light has less energy than that of the incident light, the Raman shift is called the Stokes shift. When the scattered energy is higher than incident energy, the shift is called anti-Stokes shift. Figure 4.7a shows the optical arrangement of a typical Raman spectrophotometer. When a monochromatic light (preferably Laser) is incident on the sample, the inelastic scattered Raman signals are captured by blocking the prominent Rayleigh scattered signal using notch filters. The received signals are processed through a grating monochromatic prior to recording at the detector. In the present thesis work, Raman spectrophotometer (Make: Nomadic, Model: BaySpec, USA) was used as shown in figure 4.7b with an excitation wavelength of λ=532 nm, in the range of 800-1800 cm^{-1}.

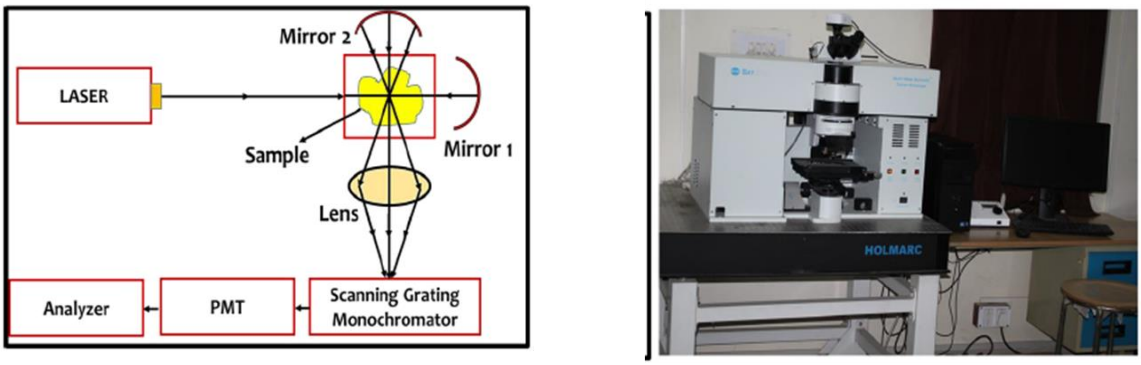

Figure 4.7: (a) Schematic for optical design of Raman Microscope (Source: Schrader, 1995) (b) Nomadic Raman spectrophotometer (Make: BaySpec, USA)

4.3.5 UV-Vis Spectroscopy

Optical properties such as absorbance, transmittance and reflectance are studied using UV-Vis spectroscopy. UV-Vis spectrophotometer consists of light sources typically deuterium and Tungsten halogen lamp for 175-1100 nm wavelength. A monochromator is used to separate all the wavelengths. The monochromatic light thus obtained is allowed to pass through the sample under investigation. Monochromatic light of intensity I_0 is allowed to incident on the sample and transmitted intensity is I; transmittance can be obtained from Beer-Lambert Law

$$T(\%) = \frac{I_0}{I} * 100$$

and absorbance is $$A = -log_{10}T$$

The diffused reflectance R is used to calculate the band gap of sample material using Davis and Mott's relation;

$$F(R) * h\nu = B(h\nu - E_g)^{1/n}$$

Where F(R) is Kulbeka-Munk function (Paul and Munk, 1931; Roy Choudhury, 2014) defined as

$$F(R) = \frac{(1-R)^2}{2R}$$

is calculated to estimate bandgap E_g using (n=2 for direct transition, B is constant). A graph between $(F(R)*h\nu)^n$ and energy, known as Tauc Plot is used for bandgap determination. Here, n=2 is for a direct bandgap and ½ for an indirect bandgap material. Here, h is Planck's constant and ν is the frequency of the incident photon. The linear region of the Tauc plot touching the X-axis gives the value of the bandgap. In our studies, we used Analytical Jena, Specord S900 Photodiode array spectrophotometer for absorbance and transmittance (figure 4.8 a&b) and Perkin Almer Lamda-900 UV-Vis-NIR spectrophotometer for diffused reflectance measurement (figure 4.8 c&d). Specord S900 is a single beam spectrophotometer. Perkin Almer Lamda-900 is a dual beam-based spectrophotometer with Deuterium and Halogen lamps as a light source. It is equipped with an integrating sphere for diffused reflectance measurements in the wavelength range 175-3300 nm. It uses a monochromator with holographic grating ~1440 lines/mm in UV-Vis and 360 lines per mm in NIR.

(a)

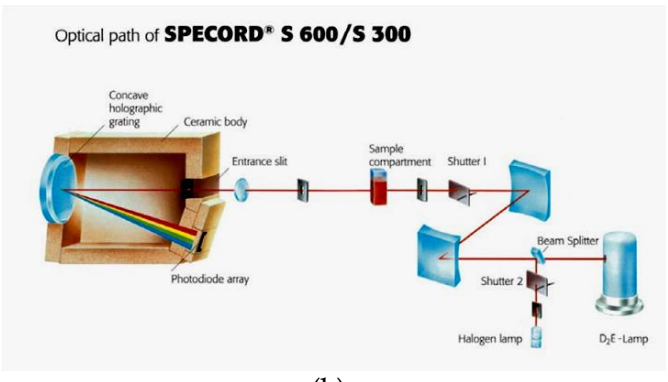

(b)

(c)

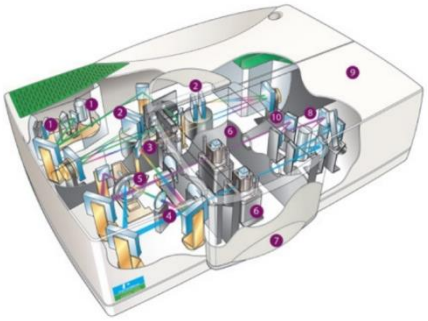

(d)

Figure 4.8: System used for UV-Vis spectroscopy (a) Specord S 900 and (b) Optical Design (Source: http://www.bds-cy.com/) (c) Perkin Elmer Lamda-900 Spectrophotometer and (d) Optical Design (Source: https://www.perkinelmer.com)

4.3.6 I-V Characterization

` I-V measurements on Gamma radiation-exposed TiO_2 samples are measured using Keithley 2636 Source Measure unit (figure 4.9). It is a device used for multiple functions such as power supply, digital multimeter, current source, electronic load and pulse generator in form of a tightly coupled highly synchronized instrument. Using this device, voltage and current can be precisely measured simultaneously in 100bV-3kV for voltage and 100fA to 50A.

Figure 4.9: Keithley 2636 Source Measure unit used for I-V characterization

4.3.7 Radiation Sources

4.3.7.1 Alpha Sources

For alpha radiation measurement, point sources of alpha radiation such ^{241}Am, ^{239}Pu and $^{241}Am+^{239}Pu$ sources were used. These sources are electroplated on a metal surface. A typical ^{239}Pu source is shown in figure 4.10.

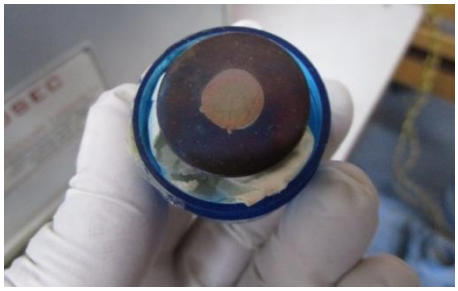

Source	Half Life	Activity
$^{241}Am+^{239}Pu$	421 years	13 Bq
^{241}Am	421 years	3700 Bq
^{239}Pu	24,100 years	22200 Bq

Figure 4.10: ^{239}Pu alpha radiation Source

4.3.7.2 *Neutron* Source

Neutron radiation measurements were performed using a 1Ci ^{241}Am-Be neutron source. Am-Be neutron source consists of $^{241}Am_2O_3$ powder mixed with metal beryllium powder. The mixture is compacted and sealed in a vacuum melted steel enclosure (figure 4.11a) (Saeed et al., 2016). Alpha particle reacts with beryllium atoms resulting in the production of neutrons;

$$^{4}_{2}He + ^{9}_{4}Be \rightarrow ^{12}_{6}C^{*} + ^{1}_{0}n$$

Neutron emitted from this reaction has a broad energy spectrum ranging from a few keV to 11 MeV with average energy ~4.2 MeV(figure 4.11b) (Marsh et al., 1995). The product nucleus carbon is often in an excited state which relaxes with emission of gamma photon~4.44 MeV

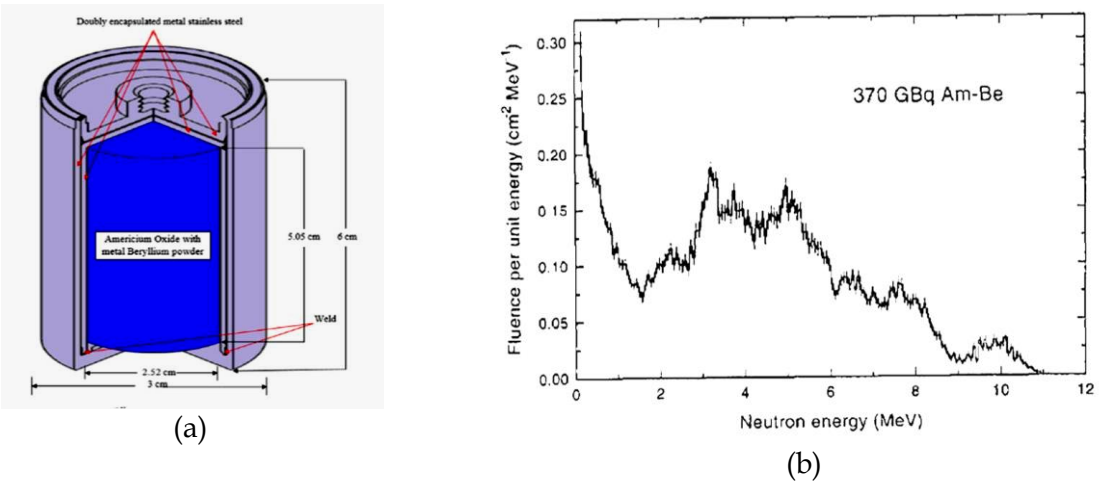

Figure 4.11: (a) Structure of Am-Be neutron Source (Saeed et al., 2016) (b) Neutron energy spectra of Am-Be neutron source(Marsh et al., 1995)

4.3.7.3 *Gamma Sources*

Gamma radiation exposures were performed in NABL accredited ^{60}Co Gamma Test and Calibration facility (figure 4.12). The facility consists of a ^{60}Co ~20 Ci capsule placed on the tip of flexible wire inside a hollow pipe housing. Source is initially stored in a depleted uranium housing which is attached to the Lead Collimator through an open pipe. Sample can be placed in front of the lead collimator on the top of the bench, moving in x, y and z-direction along with angular movements. By variation of the collimator to sample distance, various exposure rates can be varied. After placing the source at the desired place, the source is remotely controlled from another room separated by the source room by a thick wall. Unfolding the control wire leads the capsule to reach in the collimator and expose the sample for desired time.

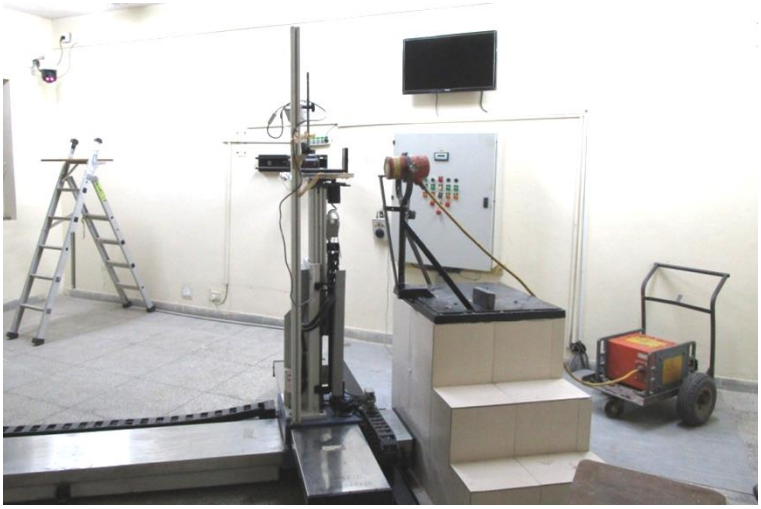

Figure 4.12: NABL Accredited Gamma Radiation Testing and Calibration Facility (DL, Jodhpur)

4.3.8 Scintillation Measurement

Interaction of radiation with scintillator material generates a light pulse in UV/Vis range. The intensity of light generated is very weak, hence cannot be detected by bare eyes. To detect this, a photosensor device with associated electronics for processing the signal is required, shown schematically in figure 4.13. These light pulse intensities can be counted using a photosensor that converts light pulse into an electrical voltage pulse amplified by a preamplifier connected immediately after the PMT. The pulse is then shaped in Gaussian shape and further amplified in subsequent stages. The amplified signal may be counted using a counter that gives the information of number of pulses generated per second or fed to a multichannel analysis that analyses each pulse's pulse height and output is displayed on PC as pulse height distributions. Details of each component are described in further sections.

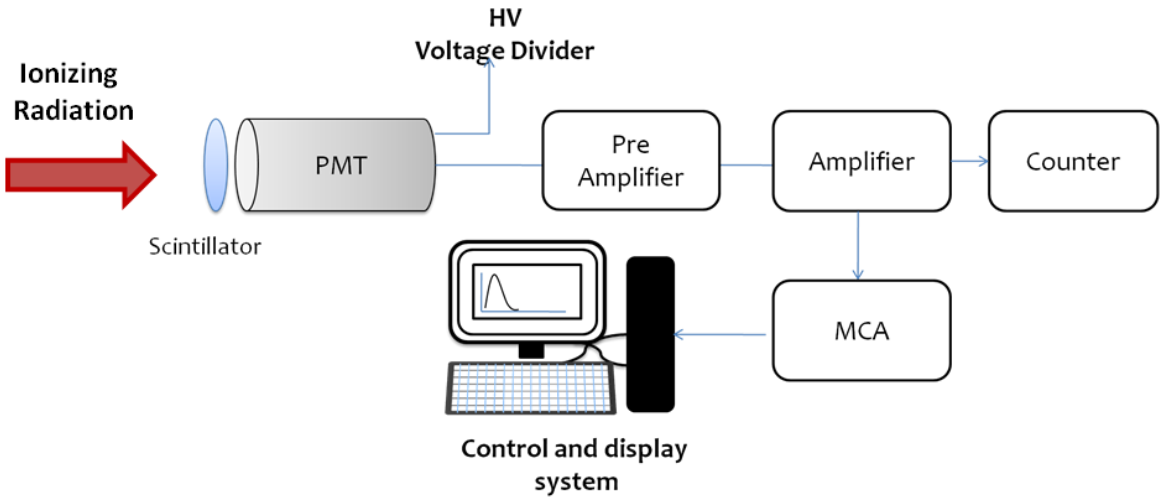

Figure 4.13: Schematics of Radiation induced Scintillation Measurement

4.3.8.1 Photo Multiplier Tube

It is a device that converts photons into electrical signal which can be processed and measured. These are very sensitive devices that are used for the detection of UV, visible and IR photons. It has application in many characterization equipment such as UV-visible spectroscopy Spectro-fluorometer, scintillation measurements and medical characterization equipment. The device uses the process of electron multiplication by different dynodes placed

between photocathode and anode at successively high potential. Radiation interacting with cathode material generates electrons which depends on the quantum efficiency of photo cathode. These generated photoelectrons, while moving towards the anode, subsequently multiplied by each dynode. The sensitivity and response of the photomultiplier tube depend on the photocathode materials, which are made of lower work function metal alloys, which produce electrons when photons fall on it due to the photoelectric effect. A schematic diagram of the photomultiplier tube is shown in figure 4.14 a and the actual PMT used in our studies is shown in figure 4.14 b.

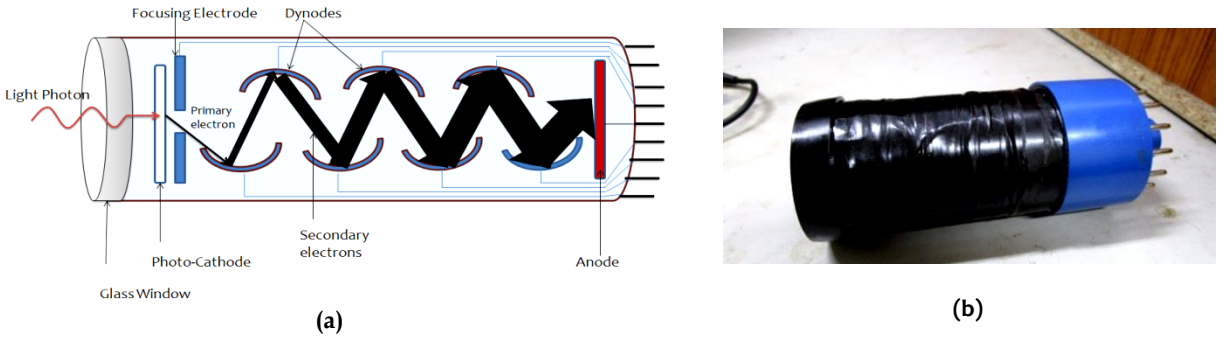

Figure 4.14: (a) Schematic diagram of Photomultiplier tube and electron multiplication (b) Actual PMT used Thorn 9256 KA used in the study (Wrapped with Black tape to protect from light)

4.3.8.2 *Pre-Amplifier*

Radiation interaction with the detector results in generation charge Q, which is generally very small, resulting in a weak pulse and needs to be amplified before any signal processing. A pre-amplifier is the device used adjacent to any detector as an intermediate amplifier for the generated pulse without reducing the signal-to-noise ratio (Ahmed, 2015). The preamplifier's output is a linear tail pulse with a very short rise time and large decay time ~50-100µs. A preamplifier is of three types: (i) Voltage sensitive, (ii) Current sensitive and (iii) charge sensitive and are explained in Fig 4.15.

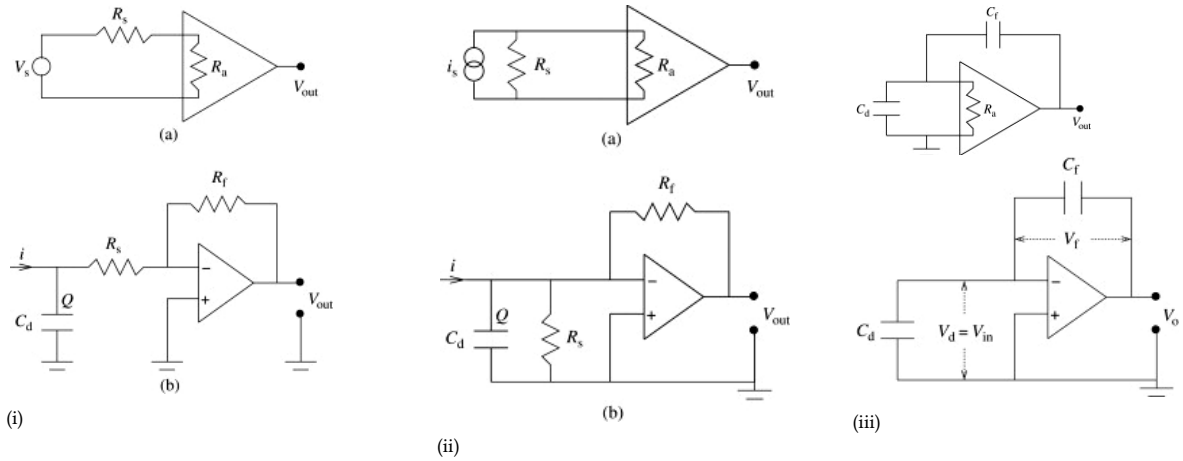

Figure 4.15: Different types of preamplifier (i) Voltage sensitive preamplifier (ii) current sensitive amplifier (iii) charge sensitive preamplifier (Ahmed, 2015)

Voltage-sensitive preamplifiers are used to amplify the signal by gain determined by the capacitance and resistance used in the design of the preamplifiers. Figure 4.15 (i) shows the

voltage-sensitive amplifier design with R_a being the input resistance, R_s source resistance, V_a voltage across the input resistance and V_S, signal voltage. These parameters are related as

$$V_a = \frac{R_a}{R_a + R_S} V_S$$

In the preamplifier, the input resistance $R_a >> Rs$, gives $V_a = V_s$. The output of voltage amplifier $V_{out} = AV_s$.

In a real amplifier, the output is given as $V_{out} = A\frac{Q}{C}$; where Q is charge collected and C is the capacitance of detector and capacitance of connecting cables. The dependence of output voltage on capacitance is problematic for detectors used in spectroscopic applications where the proportionality of V_{out} and Q should be maintained. In semiconductor detectors, any fluctuation in detector capacitance may lead to loss of proportionality between V_{out} and Q hence not used with a semiconductor detector. However, gas filled detector such as ionization chamber works effectively. Another type of preamplifier is the current sensitive preamplifier, similar to a voltage sensitive amplifier with low input resistance R_a; this allows the current to pass through the preamplifier (figure 4.15 ii). This amplifier converts the instantaneous current into voltage. The output of this amplifier is; $V_{out} = Ai_s$ and decay $\tau_d = R_sC$ is required for instantaneous conversion of the current into voltage.

The third type of preamplifier is charge sensitive. This preamplifier utilizes a feedback capacitor C_f to accumulate charge, detector capacitor C_d acting as an integrator of charge (figure 4.15 c). The output of charge-sensitive preamplifier V_{out} is proportional to Q_f/C_f or Q_d/C_f. The charge integrated at feedback capacitor Q_f is proportional to charge accumulated on detector capacitance C_d, only when current passed in R_s is negligible. Thus, charge sensitive preamplifier has infinite input impedance. Two important parameters of a charge-sensitive preamplifier are (i) charge gain A_Q and (ii) charge transfer efficiency η_{in}.

$$A_Q = \frac{V_{out}}{Q_{in}} \approx \frac{1}{C_f}$$

$$\eta_{in} = \frac{Q_{in}}{Q_{in} + Q_d} = \frac{1}{1 + C_d/C_{in}}$$

The above two equations suggest that for significant charge gain, C_f to be kept smaller and for $\eta_{in}=1$, i.e., 100%, $C_d << C_{in}$ or $C_d << (A+1)C_f$; A being the preamplifier gain. For continuous measurement, the charge integrated by feedback capacitance must be discharged to allow accumulated charge integration in the next event. This is achieved by the resistive feedback mechanism shown in figure 4.16

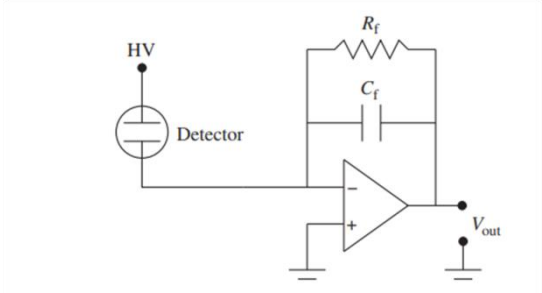

(a)

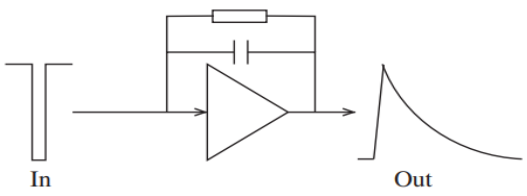

(b)

Figure 4.16: (a) Schematic of resistive Feedback mechanism in charge sensitive preamplifier (b) Exponential decay of output pulse (Ahmed, 2015)

The output of the preamplifier decays exponentially as $V_{out} = \frac{Q_f}{C_f} e^{-t/R_f C_f}$; depending on time constant R_fC_f, which can be chosen as per the requirement.

4.3.8.3 Pulse Shaping

For pulse height measurements, the preamplifier's output is not suitable as the width of the pulse is very small. Shaping is used to make the rounded top and to improve the signal-to-noise ratio. This is done by using a combination of filters CR and RC filters. Two types of circuits used for shaping applications

(i) CR-RC Shaping: this is the basic type of shaping where signal-to-noise ratio improvement is not required. It utilizes a combination of differentiator and integrator for changing the shape of preamplifier output. Figure 4.17 shows the schematic of the CR-RC shaping circuit and its output. The output of the CR-RC shaping circuit can be written as;

$$V_{out} = \frac{V\tau_1}{\tau_1 - \tau_2}(e^{-t/\tau_1} - e^{-t/\tau_2})$$

where V is the amplitude of step voltage at t=0, $\tau_1$and τ_2 are time constant for differentiator and integrator

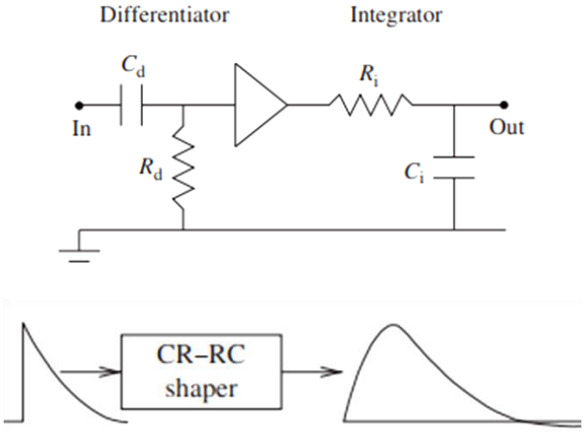

Figure 4.17: Schematic of CR-RC shaping and output pulse(Ahmed, 2015)

Typically, differentiation and integrator have the same time constant in such cases,

$$V_{out} = \frac{Vt}{\tau} e^{-t/\tau}$$

(ii) Semi Gaussian shaping (CR-RC-CR): For applications requiring high resolution and improved signal-to-noise ratio, CR-RC-CR shaping is used. The schematics of CR-RC-CR are shown in figure 4.18 and its output for a step input.

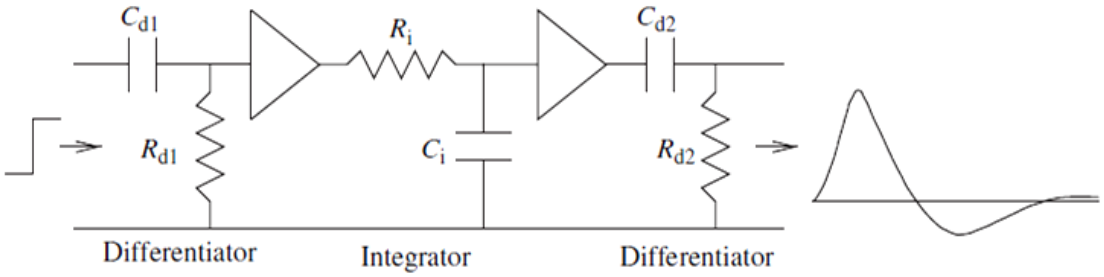

Figure 4.18: Schematic of CR-RC-CR shaper and output for step input (Ahmed, 2015)

The output of CR-RC-CR is bipolar, which minimizes the base lift is obtained in CR-RC shaping, but the bipolar output may reduce the signal-to-noise ratio, to make it unipolar in two stages of CR-RC-CR is used.

4.3.8.4 Multi-channel Analyser

A multichannel analyzer is a device used for the analysis of voltage pulse height distribution obtained from PMT. The output of the preamplifier and shaping amplifier is fed to MCA for analysis of the height of the pulse. It utilizes an analog to digital conversion circuit for converting the analog signals into a digital pulse and a memory for storage of the digital pulse. A schematic of MCA is shown in figure 4.19.

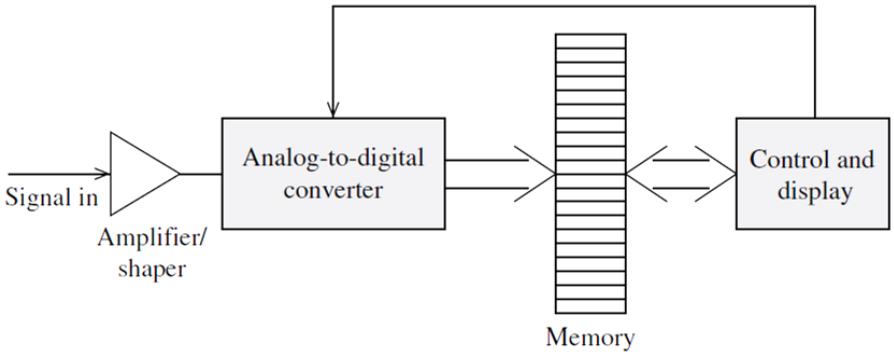

Figure 4.19: Schematic diagram of the multichannel analyser (Ahmed, 2015)

An analog to digital converter (ADC) is a device, which converts information in analog form to a digital equivalent that can be saved in memory. The performance of an ADC is governed by various parameters such as conversion time, dead time, resolution, linearity and stability. Conversion time is the time consumed by ADC in converting the signal from analog to digital. It depends on the conversion method and height of the pulse for which conversion is required. Deadtime refers to the time between two ready states of ADC in which it is unable to process the signal. It includes acquisition and conversion time, data transfer time and reset time. The resolution of ADC is the minimum height of the pulse, which can be assigned a digital number. For n bit ADC, resolution ~ $1/2^n$. The higher the number of bits, high will be the resolution. The output of ADC should be linear to the input signal. Nonlinearity should be removed or minimized for high-resolution systems. Any change in physical parameters on which A/D is dependent may change the performance of ADC and is not desirable.

Many analog-to-digital conversion methods are performed, such as Digital ramp ADC, Successive approximation ADC, Tracking ADC, Flash ADC and Wilkinson ADC. In Our MCA,

Wilkinson ADC is used. This ADC utilizes a pulse stretcher circuit that stretches the input pulse and is used to charge a memory capacitor. After charging, the memory capacitor is allowed to discharge linearly using a constant current source. The duration of the discharge is monitored by the counter with a clock. Time taken in complete discharge of the capacitor is defined as

$$t_d = V_{in}\frac{C}{i_s}$$

Discharge time is proportional to the digital counter. Hence, the digitized output is proportional to the input voltage. Figure 4.20a shows the schematic diagram GSpec USB 1kMCA with different inbuilt components and figure 4.20 b shows the actual GSpec USB 1k MCA used in our scintillation measurement

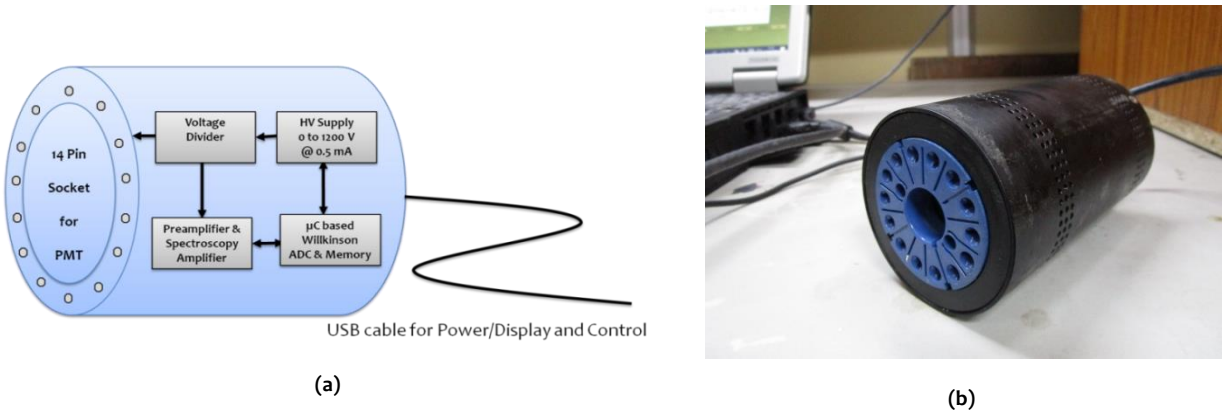

(a) (b)

Figure 4.20: (a) Block diagram GSpec-USB MCA (b) Actual multichannel analyser used in the study

4.4 Measurement of Radioactivity

Radioactivity is the disintegration of unstable atoms per second, releasing radiation such as alpha, beta, gamma and neutron. These radiations, when interacting with detector materials, particularly the scintillator it produces light. These light pulses were measured in the form of counts. Two important parameters of a radiation detector are detection efficiency and minimum detectable activity (MDA).

4.4.1 Detection Efficiency

Absolute detection efficiency is defined as the ratio event registered in the detector divided by the total events emitted from the source (Leo, 1994).

$$\varepsilon = \frac{Events\ registered\ (Net\ Counts)}{Events\ emiited\ from\ source\ \ (Activity)}$$

4.4.2 Minimum Detectable Activity (MDA)

Radiation measurement using pulse height analysis is obtained using count measured above background. If the background has fluctuations, a confidence limit must be set for ascertaining that count obtained are real counts obtained due to radiation source.

Net counts obtained by difference of counts from the unknown sample (N_T) and blank sample without radiation source (N_B);

$$N_S = N_T - N_B$$

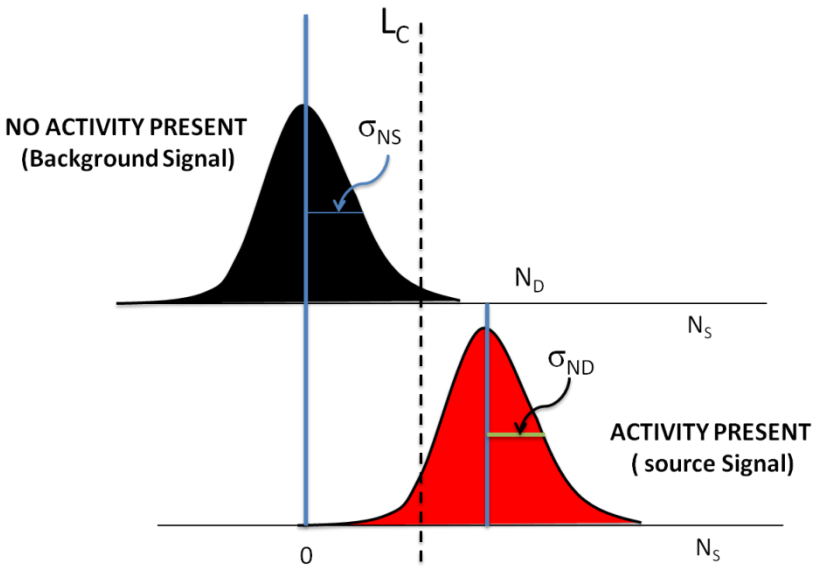

Figure 4.21: Distribution of Net Counts when no activity is present (upper) and when activity is present (lower)

A critical level L_C is set and comparing the net counts N_S with L_C, the decision is made whether the sample contains activity or not depending upon $N_S < L_C$ or $N_S > L_C$. L_C is set high enough to minimize false positives (figure 4.21). For a large no of counts, N_s can be treated as Gaussian distribution. When no activity is present, then for 95% confidence that N_S will be below L_C, then L_C can be set as

$$L_C = 1.645 * \sigma_{N_s} = 1.645 * \sqrt{2}\, \sigma_{N_B} = 2.326\, \sigma_{N_B}$$

When a real activity is present, N_s is greater than L_C. Let N_D be the net value count which is high enough and represent a real positive; for 95% of the area of N_S falling above the L_C then,

$$N_D = L_C + 1.645\, \sigma_{N_D}$$

$$\sigma_{N_D} = \sqrt{2}\, \sigma_{N_B} + 1.645$$

Then,

$$\mathbf{N_D = 2.71 + 4.66\, \sigma_{N_B}}$$

This is an expression for minimum counts above the background, which can be said to be positive with 95 % confidence.

The minimum detectable activity (MDA) can be obtained by dividing the minimum detectable counts by detection efficiency and time

$$MDA = \frac{N_D}{\varepsilon * t} = \frac{2.71 + 4.66\sqrt{N_B}}{\varepsilon * t}$$